IEEE Access
Multidisciplinary | Rapid Review | Open Access Journal

Received April 29, 2021, accepted May 5, 2021, date of publication May 10, 2021, date of current version May 18, 2021.

Digital Object Identifier 10.1109/ACCESS.2021.3078532

Design and Development of Low Cost, Portable, On-Field I-V Curve Tracer Based on Capacitor Loading for High Power Rated Solar Photovoltaic Modules

JAVED SAYYAD AND PARESH NASIKKAR

Department of Electronics and Telecommunication Engineering, Symbiosis Institute of Technology, Symbiosis International (Deemed University), Pune 412115, India

Corresponding author: Javed Sayyad (jksayyad23@gmail.com)

ABSTRACT This paper outlines a novel design of low-cost, portable, fast, and precise Current-Voltage Curve Tracer (IVCT) with automated parameter extraction for high power rated Solar Photovoltaic (SPV) modules to effectively and efficiently determine the outdoor operating status of SPV power generators. The developed IVCT is based on a Raspberry Pi microprocessor, a super-capacitive load, heat sinkable discharge resistances, and sensors with high sensitivity and resolution for measuring light irradiance, module temperature, current, and voltage. The proposed Outdoor Test Facility (OTF) consists of an Current-Voltage ($I-V$) and a Power-Voltage ($P-V$) curve tracer that uses a dynamic loading supercapacitor to safely and quickly scan the SPV module performance characteristics under real-world operating conditions. It also helps to achieve uniform sampling with better data accuracy. It uses Raspberry Pi as a central processing unit for low-cost data acquisition, data logging, and data computation. Furthermore, results from on-field testing of various small-scale SPV modules show that the $I-V$ tracer can acquire higher-resolution characteristics curves and perform accurate model parameter recognition in real-time. Proposed IVCT can measure individual SPV modules without altering the electrical interconnection circuit, and the operating point can be shifted to 20 A and 45 V in few seconds. The proposed system recomposes the SPV module $I-V$ characteristics based on this variance, with accuracies of 1 to 3% for the region near maximum power.

INDEX TERMS I-V curve tracer, capacitive load, Internet of Things (IoT), on-site $I-V$ curve measurement, solar photovoltaic.

I. INTRODUCTION

In recent years, the development of renewable and sustainable solar energy has accelerated worldwide as a source of green electricity to address issues such as fossil fuel depletion, pollution, climate change, and other concerns [1]–[5]. Solar Photovoltaic (SPV) power generation is a feasible and most widely adopted method of directly transforming sunlight into electricity for solar energy harvesting and can be implemented in residential and commercial spaces [6]–[9]. The SPV modules are the core device for SPV power generation systems expected to run outdoors for decades. However, due to the harsh outdoor environment, the SPV module's long-term viability will inevitably undergo normal aging, resulting in a gradual decrease in power efficiency [10]–[13]. The impact of incident light angle, intensity, and ambient temperature on energy harvesting performance and Maximum Power Point (MPP) estimation of SPV modules significantly impacts the system's overall efficiency [14], [15]. Identifying an ideal geographical location for solar power plants' installation is also crucial in designing a viable SPV-based power project [16]. According to the study, Non-linear degradation rates for silicon modules are usually less than 1% a year [17]. Regardless of how bright the future of solar energy appears to be, there are still several challenges to overcome, including low-performance efficiency, relatively high cost, climate dependency, and storage space [18]–[24].

The associate editor coordinating the review of this manuscript and approving it for publication was Chi-Seng Lam.

The output $I-V$ curves of SPV modules are usually obtained using the Current-Voltage Curve Tracer (IVCT) device to verify SPV arrays' electrical performance under actual operating conditions to detect anomalies and/or faults [25]–[28]. IVCT device can be used regularly to capture the $I-V$ characteristics of SPV cells, modules, strings, and arrays to see how solar irradiance and temperature affect SPV generator performance [29], [30]. Simultaneously, managing a large SPV power plant requires maintenance rescheduling and fault detection before failure, which is often needed to increase performance and reliability [31]. Based on onsite IVCT data, several researchers have investigated diagnostic strategies [32]–[34]. IVCT is a fast and accurate way to check performance and troubleshoot issues before becoming significant [35]. Many simple characteristic parameters can be derived directly from $I-V$ curves, such as open-circuit voltage (V_{oc}), short circuit current (I_{sc}), maximum current (I_m), and maximum voltage (V_m), as well as Fill Factor (FF) [36]. When these parameters are STC correlated with ambient irradiance and temperature, the SPV power generator's operating state can be evaluated. Compared to such direct parameters, internal model parameter specifics are more important for determining SPV modules/arrays' performance [37], [38]. These parameters must be extracted from data collected with $I-V$ curve tracers [39]–[42].

The SPV module's characteristics curve must be swept under uniform and non-uniform operating environmental conditions to track an SPV power generator's MPP [43]. These characteristic curves are unimodal in uniform conditions, whereas they are multimodal in non-uniform conditions [44]. Non-uniform conditions, such as irradiance variance, can be exacerbated by the sun's displacement during the day, soiling, and shadowing [45]–[48]. Nearby buildings, trees, and objects cause the Partial Shading Condition (PSC). Soiling occurs due to dirt and dust accumulation on the SPV module protective glass. It results in irreversible hot spot damage and, in severe situations, module failure [49]–[51]. Local shading, impaired cells, module mismatch, short circuit bypass diodes, reduced shunt resistance, and increased series resistance are signs of impairments seen in the characteristic I–V curve's shape [52]–[54]. Several $I-V$ curve testing methods, including the variable resistive load method [55]–[57], DC-DC loading methods [58], [59], varying electronic load methods (e-load) [56], [60]–[66], and capacitor charging dependent load methods [52], [67]–[72], have been proposed in recent years.

This study proposes a Super Capacitor load-based technique to achieve auto-sweep over other commonly used methods in the literature, allowing higher resolution data collection with adequate scan time to sweep the characteristic curve. We use the Internet of Things (IoT) in conjunction with a super capacitive load-based IVCT device's novel design to characterize high power rated SPV modules up to 900 W_p. This allows Enhanced Monitoring and Control (EMC), cost-effective data collection, interconnected computation, and power generator management for remote database logging and automatic structured measurements for quality assurance and performance determination [73], [74]. The short-term output of silicon mono-crystalline SPV modules deployed at an outdoor location is logged and evaluated using several electrical and meteorological parameter sensors integrated with Raspberry-pi microprocessor. The data points for the $I-V$ and $P-V$ curves of SPV modules are continuously and periodically swept and logged. These collected data points are stored in a local as well as remote database with an Automatic Structured Storage Strategy (ASSS) for quality assurance and success determination. The logged time-series data points are analyzed in more detail for better data visualization and interpretation with tools represented by a set of Python scripts. The captured $I-V$ curves are analyzed to evaluate the SPV modules' performance and determine the extent of degradation and the causes of failure in the field.

In this introductory section, the need for SPV-generated renewable energy is addressed with several challenges in the SPV research field. This section also focuses on the need for IoT-based smart IVCT devices for the performance monitoring and output characterization of the high power-rated SPV module in the Renewable Energy (RE) industry. Section 2 contrasts current $I-V$ curve tracing typologies and summarizes their benefits and drawbacks. The proposed capacitor charging-based IVCT device's design and implementation are addressed in Section 3 using block diagrams and step-by-step hardware integration. Section 4 demonstrates and compares the experimentally measured and STC converted data points with resistive load-based outcomes to validate the capacitive load-based method's outcomes to summarize the different reasons behind the $I-V$ curve's variation from the one provided by the manufacturer. Finally, section 5, conclusion with future research directives, are discussed.

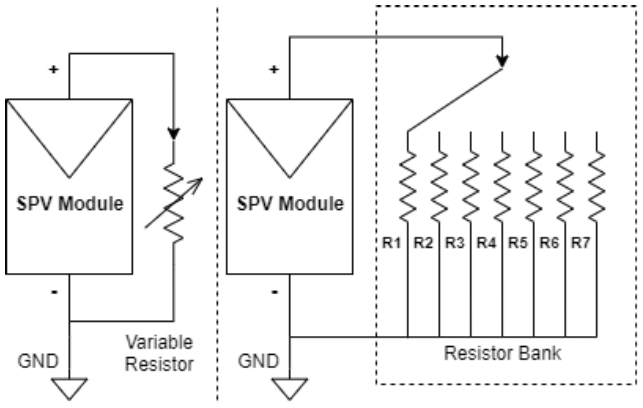

FIGURE 1. Resistive load approach.

II. OVERVIEW OF ELECTRICAL LOADING TYPOLOGIES

A. RESISTIVE LOAD METHOD

In the resistive load approach, the SPV cell or SPV module is directly linked to a variable resistor or resistive load bank for characterization, as shown in Figure 1. A manually actuated rheostats [75]–[77] or switch-controlled power resistors [78]–[80] are used to change resistance step-wise.

The SPV characterization curve's data points are logged by changing the electrical load's resistance from minimum to maximum, which helps to move the trace from a short circuit to an open circuit. Electromechanical relays are used to choose the desired resistor combination, which reduces scan time. A computer card or electronic circuitry can regulate the operating sequence of an electromechanical relay array. To ensure safe and accurate assessment, resistor power ratings are kept slightly higher than operating power. Power resistors are used to dissipate power while preventing the resistive part from overheating.

1) ADVANTAGES

- This method is simple, straightforward, economical.
- Produces noticeable results for small power-rated SPV modules characterization.

2) DRAWBACKS

- Time-consuming and labor-intensive, imprecise and rigid.
- Not suitable for non-uniform climatic conditions and practical engineering applications.
- Unable to determine the exact value of I_sc.
- A wide range of power resistors is needed to characterize high power rated SPV module, which becomes heavy, bulky, and expensive.
- Another factor to consider is the scarcity of high-power resistors.
- The sample data points on the $I - V$ curve will be limited due to the limited combination of available resistors [78].

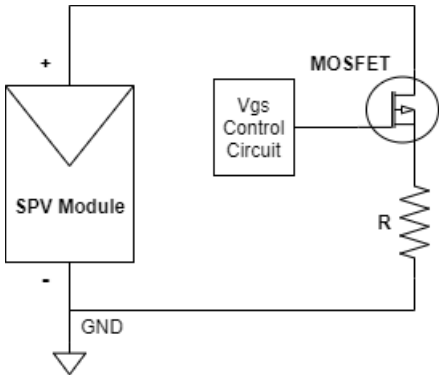

FIGURE 2. Electronic load approach.

B. ELECTRONIC LOAD

Usually, e-load methods use power transistors such as MOSFET, BJT, or IGBT [81]–[83]. When MOSFET operates in a linear (ohmic/triode) region, it emulates as a variable resistor where the resistance between the drain and the source (R_{DS}) varies with the gate-source driving voltage (V_{GS}) as shown in Figure 2. A BJT, on the other hand, is a current regulated current source that operates as a controllable impedance by gradually varying the input current ramp signal. In [84], the authors have proposed and designed IVCT using an electronic load approach with a low-cost Wireless Sensor Network (WSN) to gain the advantage of automated data logging for the distributed SPV modules.

1) ADVANTAGES

- The use of programmable microcontroller aid in the automate and accelerate signal measurements during sweep of curve [85], [86].
- Characteristic curves can be swept in any direction, from open circuit to short circuit and back again.

2) DRAWBACKS

- MOSFETs exhibit a finite value of $R_{DS(on)}$ in the saturation region, resulting in incorrect measurement near I_{sc} [87].
- MOSFET cannot generate I_{DS} in the cut-off region, resulting in incorrect measurement near V_{oc} [87].
- Transistors are only used for low power rating SPV module characterization since they can only hold high power for a few milliseconds as a load.
- When it comes to high power ratings, a heat sink and cooling fans are needed for safe operation [87], [88].
- Due to the non-negligible influence of the parasitic, capacitive, and inductive MOSFET parameters, measuring error occurs [89].
- The gate capacitance (C_g) of MOSFETs is high, and it should be charged above the threshold voltage (V_{th}), necessitating an additional Gate Driver Circuit (GDC), which provides high output current to charge gate capacitance quickly [89].

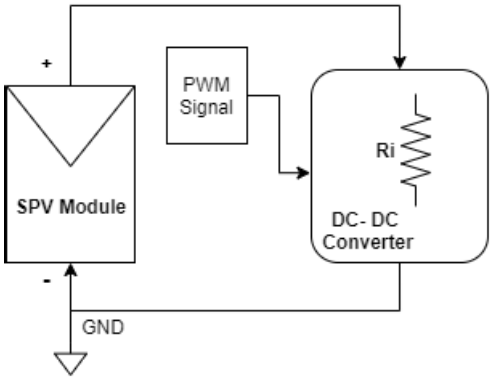

FIGURE 3. DC-DC converter load approach.

C. DC-DC LOAD

For SPV modules' characterization, the DC-DC converter (chopper), which emulates as a loss-free variable impedance, is used to trace the curve from a short to open circuit and vice-versa [90], [91] Figure 3 shows that a DC-DC converter can shift the DC voltage's magnitude up or down and/or reverse the polarity using an electronically generated PWM signal with a constant frequency, and variable duty cycle (D) from 0 to 1 [92]. In [93], author have characterized the output

performance of SPV module by analyzing and simulating a programmable buck converter with IGBT-based switching. In [94], portable IVCT is proposed by the author, which is based on the DC-DC Ćuk converter for the characterization of SPV modules of up to 300 W_p. In [95], the authors have used Source Meter Unit (SMU) controlled by MATLAB software, which emulates as DC-DC load-based IVCT with electromechanical relay switching to sweep the characteristic curve of small scale SPV module. The microcontroller-based electronic circuit is used to control the duty cycle of the PWM signal, which speeds up the operation, resulting in a shorter overall scan time and more evenly distributed data points on the characteristic curve [96].

1) ADVANTAGES

- Can sweep in both directions from short circuit to open circuit and vice versa.
- In rapidly changing irradiance and PSC, this method provides a high degree of stability.

2) DRAWBACKS

- Buck and Boost DC-DC converters cannot measure values near I_{sc} and V_{oc} of the SPV module, respectively.
- It cannot control duty cycle above 80 percent leads to error in measurement.
- It will take some time to complete the characteristic curve sweep, which causes power sinking during operation [97].

D. BIPOLAR POWER SUPPLY

In this approach, a Class-B power amplifier is used as a load, with two BJTs handling forward and reverse current. BJTs must function in the cut-off, active, and saturation regions for best performance. It employs two complementary transistors (NPN and PNP), each receiving the same control signal of equal magnitude but opposite phase. Initially, the complementary pair of BJT's operating points are located in the cut-off region. The function generator is used as a stepped voltage source in conjunction with a DC power amplifier to provide the high test current required by the SPV cell or SPV module. Artificial light is used as a solar simulator combined with an automatic setup based on a computer-connected standard GPIB instrument to characterize the SPV module. The operator will measure and log current and voltage values using individual digital multimeters.

1) ADVANTAGES

- A programmable microcontroller aids in the accurate sweep of a characteristic curve.
- The characteristic curve can be swept in all directions, from short to open circuit and vice versa.

2) DRAWBACKS

- During operation, the power delivered by the SPV cell or SPV module must be dissipated by BJTs, limiting the use of load to medium power.
- The use of a heat sink to dissipate heat makes the device bulky and expensive.

E. FOUR QUADRANT POWER SUPPLY

A four-quadrant power supply is one whose output can be varied by a reference input signal or designed to sweep a specific set of values. this approach is capable of supplying (current source) and dissipating (current sink) power. Voltage and current values will be positive or negative, allowing the power source to be used in all four quadrants. The voltage sweep of the power supply can be regulated electronically using a microcontroller or microprocessor. In this approach, A manual step-wise minor shift in bipolar transistor's operating point and power supply voltage leads to a change in load resistance from open circuit to short circuit condition [55]. The SPV module's $I - V$ curve is in the first quadrant. However, extrapolation near short circuit current and open circuit voltage causes data points to scatter into the second and fourth quadrants, respectively, which aids in detecting potential loss and mismatching. A four-quadrant power supply is used to mimic real-world load characteristics when measuring and analyzing DC power supplies and other DC output voltage sources such as a fuel cell, batteries, SPV generators, and so on.

1) ADVANTAGES

- A sweeping characteristic curve in all quadrants provides valuable information about the performance of the SPV module.

2) DRAWBACKS

- This form of power supply is costly and difficult to design.

F. CAPACITIVE LOAD

On the other hand, the capacitor loading approach uses the capacitor's emulation property as a variable resistor. When the SPV module's DC output voltage is applied to the capacitor, the capacitor's charge increases, the amplitude of the current decreases, and the voltage gradually rise. This method charges the capacitor passively until it exceeds open-circuit voltage and records the characteristic curve's data points. It employs many high-voltage capacitors connected to active switches to meet various I–V monitoring requirements as the load changes [98], [99]. Since the capacitors' terminal voltage does not change suddenly and grows progressively as the charge increases, the output $I-V$ curves from I_{sc} to V_{oc} can be obtained automatically during the capacitor charging phase.

Figure 4 depicts a typical measuring circuit used in this typology-based system. In [100]–[104], the authors have proposed the main circuit and hardware prototypes for a capacitive load-based system. The instantaneous voltage and current values are obtained directly by connecting the SPV module's terminals to the capacitive load through the S1 switch. After completing the measurement, any heat sinkable component, such as a resistor, is connected using the

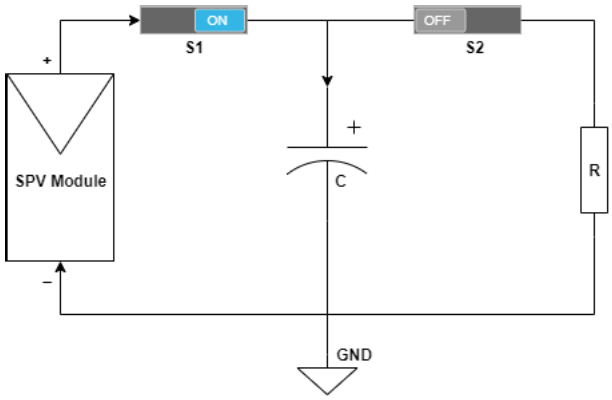

FIGURE 4. Capacitor loading approach.

S2 switch, which is used to discharge the capacitor charge. In [105], authors have used electrolytic capacitor based load to characterize 5 *Wp* SPV module, which is controlled by the microcontroller.

In the literature [67], [70], [106], [107], several authors have suggested formulas to determine the scan time for a capacitive load-based approach to sweep the $I - V$ curve from I_{sc} to V_{oc}, which is a very short run. Capacitors used in measurements may be sized to match the measurement time and resolution required. Furthermore, since capacitors primarily store electric charges and consume very little power, this method is reliable and safe. This method is versatile and practical enough to provide accurate and better results when partial shading condition occurs, or the weather is rapidly changing. This loading approach also assists in recognizing global and local MPP [108], [109]. This method offers natural sweep with reduced voltage and current ripples during measurement and accurate and precise I_{sc} and V_{oc} values during characteristic curve trace. This method is used by the majority of commercially available $I - V$ curve tracers for small power-rated SPV modules to high power-rated SPV arrays that make this method scalable. To capture characteristic curves of different SPV modules, the capacitor used in IVCT must cover a wide range of capacitance, voltage, and inrush current, using bulky and costly capacitors for tracing.

1) ADVANTAGES

- With changing irradiance conditions and in PSC, there is a high degree of versatility [109].
- Measurements of I_{sc} and V_{oc} with minimum error and ripple.

2) DRAWBACKS

- Requires additional discharge circuitry to dissipate stored charge of the capacitor safely.
- A high-quality electrolytic capacitor with a low Equivalent Series Resistance (ESR) is expensive.
- For the characterization of high power rating SPV cells or SPV modules, the size of the capacitor becomes large and bulky.

III. DESIGN AND DEVELOPMENT OF PROPOSED CAPACITOR CHARGING BASED IVCT

This section focuses on the device architecture of the proposed IVCT and the components and sensors used in the design. The detailed block diagram, electronic component-based block diagram, and electronic component circuit connection diagram of the conducted experimental setup of the proposed IVCT for the SPV module are shown in Figures 5, 6, and 7, respectively.

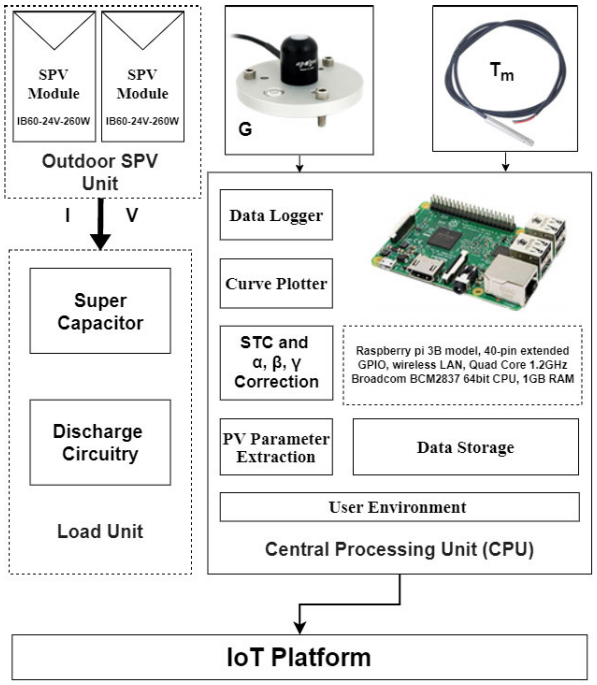

FIGURE 5. Detailed block diagram of proposed capacitor load based IVCT.

The outdoor performance characterization is routinely monitored under variable load conditions using the proposed capacitive loading topology-based IVCT configuration for the SPV power generator. To acquire characteristic curves, the load impedance changes from I_{sc} to V_{oc} in a very short amount of time. Sweeping the curves in a continuously changing climate and environment is challenging [110], [111]. The SPV module generates active energy, while the IVCT acts as a load, sweeping the characteristic curve with internal load circuitry. The SPV module is directly connected to the supercapacitor through an electromagnetic relay switch managed and controlled by a Python script. It causes the capacitor charge current to increase to track the curve trace from no resistance to infinite resistance direction by simulating as a variable resistance. The outdoor SPV unit, Sensors unit, Load Unit, and Central Processing Unit (CPU) are the primary building blocks for the proposed IVCT design.

The outdoor SPV unit performs the function of Device Under Test (DUT). Voltage Divider Circuit (VDC), ADS712, SP-110-SS pyranometer, and DS18B20 sensors are used in the sensor unit to measure voltage, current, light irradiance,

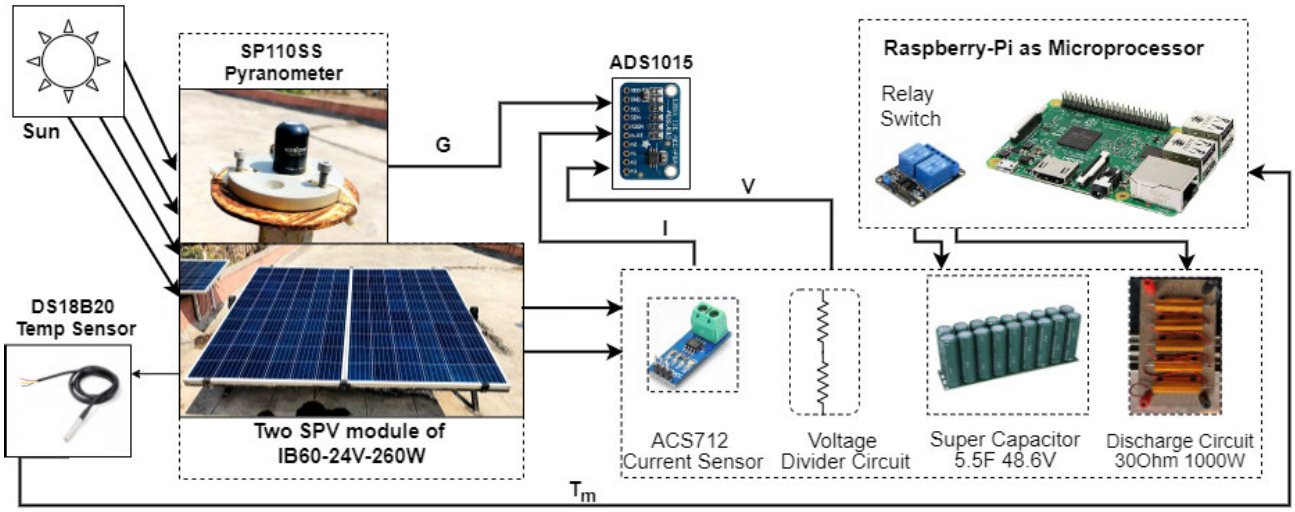

FIGURE 6. Electronic component based block diagram of IVCT design.

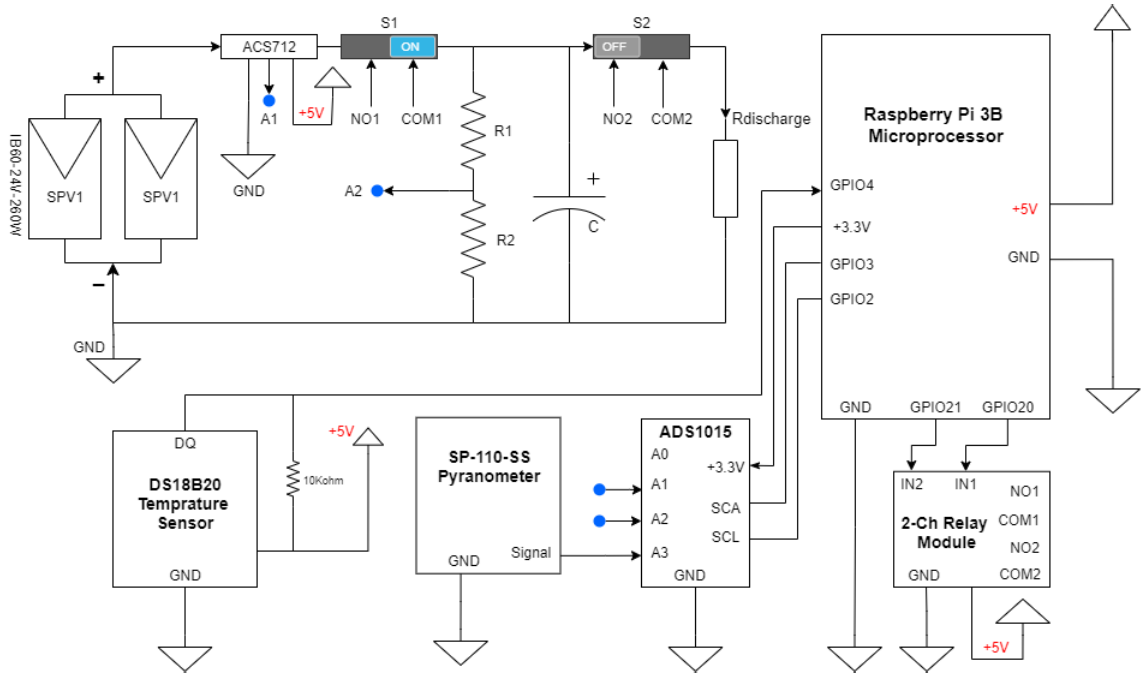

FIGURE 7. Electronic component circuit connection diagram.

and module temperature, respectively. The load unit comprises a super capacitor-based electrical load and a heat sinkable resistor-based discharge circuitry. A single small board of Raspberry-Pi 3B microprocessor computer serves as a CPU for data logger, curve plotter, STC correction, SPV parameter extraction, and data storage. The CPU also acts as a data acquisition, data logging, and data computation application. The proposed IVCT's measurement ranges and some specifications are shown in Table 1.

A. OUTDOOR SPV UNIT

For the experimentation, two silicon mono-crystalline SPV modules are considered as a DUT in this study. It has a power rating of 260 W_p each, installed on the SPV laboratory's terrace for IVCT research. These SPV modules are connected in parallel, offering the total maximum output power of 520 W_p. For this experiment's validation purpose, the SPV module has been mounted on the outdoor location, as shown in figure 8. The geographical location information and the

TABLE 1. Measuring ranges and some specifications of the developed IVCT.

Measuring ranges	
Voltage	45 V
Current	20 A
Module Temperature	-55 °C to +125 °C
Light Irradiance	1500 W/m^2
Display	
7" touch screen display. Resolution: 800 x 480 Pixel. 10 finger capacitive touch. On-screen virtual keyboard.	
Operations	
Raspbian OS. Set of code written in Python.	
Power Supply	
Triple port output. 20000 mAh lithium polymer battery continuous operation > 6 hours.) Inbuilt 12 layer chip protection for power bank charging. 18 W lightning charging. Four LEDs at the front panel to display power bank's charging status.	
Dimensions	
W x H x D : 30.48 cm x 12.7 cm x 30.48 cm Weight: 2.5 kg	

FIGURE 8. 520 W_p SPV module as DUT.

electrical specification at Standard Test Condition (STC) with other mechanical specifications provided by the manufacturer are shown in Table 2.

B. LOAD UNIT

The load unit consists of a super-capacitor as an electrical load with the heat sinkable components as a discharge circuitry to ensure safety.

1) SUPER CAPACITOR

After investigating the most appropriate load resistance typologies [112]–[116], the capacitor-based load approach is selected to obtain the SPV module's $I-V$ curve. This method is also generally used for most of the available commercial IVCTs. A capacitor offers a low resistance path during charging and an infinite resistance path after capacitor voltage equals the SPV module DC output voltage. It will help trace the $I-V$ curve naturally, automatically, and precisely with minimal voltage and current ripple [117]. There are several types of capacitors available, but they can differ depending on

TABLE 2. On-site mounted SPV module characteristics.

On-Site Location Details	
Location	SIU, Pune, India
Module Make	Integrated Batteries India Pvt. Ltd.
Model	IB60-24V-260W
Type of Module	Mono-crystalline
Number of Modules	2
Total Output Power	520 W_p
Tilt Angle	18°
Azimuth	180° (Facing South)
Installation Type	Roof Top Mount
Latitude	18°32'27.9" N
Longitude	73°43'43.2" E
Electrical Data at STC	
V_{mp}	30.9 V
I_{mp}	16.84 A
V_{oc}	37.7 V
I_{sc}	17.78 A
P_m	520 W_p
N_s	72
η	16.01 (%)
Temperature Coefficients	
β	−-0.0031 (°C)
α	0.000402 (°C)
γ	−0.00426 (°C)
Mechanical Data	
Dimension (L × W × H) mm	1335 × 987 × 40
Surface [m^2]	1.318

the type of task to be performed. While selecting capacitors for electrical load, specific criteria need to consider for safety and measurement accuracy. The capacitors voltage rating should be at least 15% higher than the SPV module output DC voltage. The capacitor's selection is also influenced by the voltage variance parameters, the load's transient amplitude, and the capacitor's impedance. Other essential selection factors to be considered includes availability, cost, and minimizing the PCB area. Table 3 shows the maximum possible capacitance, voltage rating, operating temperature range, and applications of various types of capacitors. Aluminum Electrolytic Capacitors (AEC) or supercapacitors are best suitable as an electrical load in IVCT device as they have low tolerance, better low-frequency characteristics, and are available in a broad range with low equivalent series resistance (ESR). Figure 9 shows the actual electronic circuit topology design used in the proposed IVCT.

2) DISCHARGE CIRCUITRY

After tracing the $I-V$ curve, the heat sinkable component must discharge the charged capacitor ultimately to begin the new sweep cycle without any initial error. It can be accomplished by switching OFF charge switch S1 and switching ON discharge switch S2. Here two-channel 5V operated electromechanical relay is used as a switch. These switches' timing and operation are taken care of by the python script and the Raspberry pi microprocessor. Any heat sinkable like a resistor, rheostat, or light bulb can be used for this task. The initial requirement for selecting any component as a discharging element is to withstand the voltage stored in the capacitor.

TABLE 3. Capacitor type comparison.

Type of the Capacitor	Max. possible Capacitance	Voltage range	Max. operating Temperature (°)	Applications
Aluminum Electrolytic Capacitor (AEC)	< 1F	600V	85 to 150	DC buffering, DC/AC, AC/AC converter >500W, Frequency converter, Smoothing, DC Link
Film Capacitor	< 1mF	3 kV	Max 110	Timing, Snubbing, S/H ADC, TV flyback tunning, Peak voltage detector, DC link
Multilayer ceramic chip capacitors (MLCC)	< 100 uF	10 kV	85 to 200	HF coupling/blocking, DC-DC convertor, EMI suppression, HF decoupling/ bypassing
Super Capacitors	< 1 kF	10 V	85 to 150	EMI suppression, Smoothing, Coupling, By-passing, Blocking

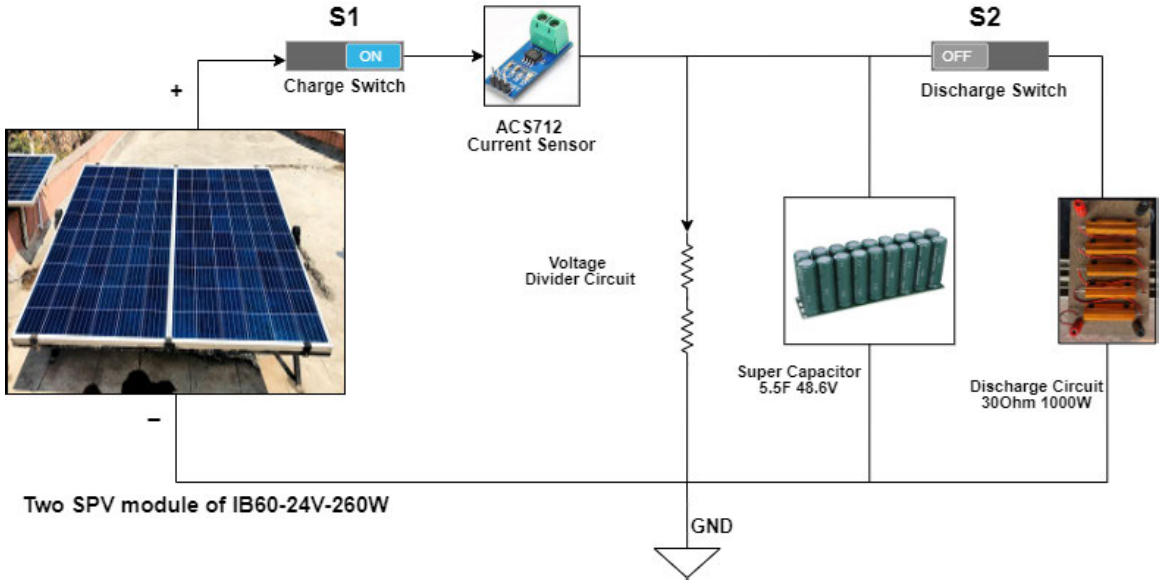

FIGURE 9. Electronic circuit topology design for IVCT.

The discharge element's power rating is also vital to discharge the capacitor safely in the shortest time possible.

In This study, Aluminum Housed Heat Sinkable Resistors (AHHSR) are connected parallelly to design the resistance bank, which assimilates heat during capacitor discharge and releases it into the air. Five identical AHHSR of specification 300 Ω, 100 W each are connected in parallel, having equivalent resistance 60 Ω 500 W as shown in figure 10. The pair of this type of topology is connected in shunt to get a 30 Ω 1000 W equivalent resistance. Equation 1 specifies the minimum time required to safely discharge the capacitor [107], where τ is the maximum time the capacitor requires to discharge, R_{eq} is the equivalent resistance of discharge circuitry, and C is the capacitance's value in the electrical load circuitry.

$$\tau >= 5 * R_{eq} * C \tag{1}$$

C. MEASURING SENSORS

The proposed IVCT is designed to trace 520 W_p SPV module performance characteristics considering SPV cell temperature and light irradiation during the measurement.

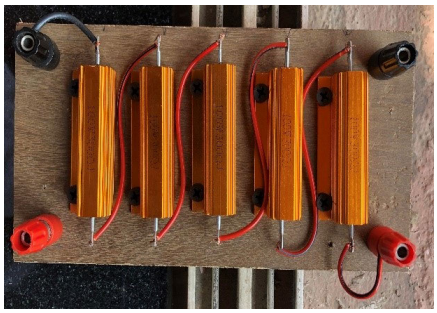

FIGURE 10. Aluminum housed heat sinkable resistors (AHHSR) are connected parallelly.

The sensor unit comprises different sensors like Voltage Divider Circuit (VDC), ADS712, SP-110-SS pyranometer, and DS18B20 for voltage, current, light irradiance, and module temperature measurement, respectively.

1) TEMPERATURE MEASURING

A DS18B20 digital thermometer uses a single wire serial communication protocol for communication with a central

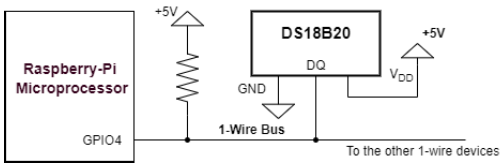

FIGURE 11. DS18B20 with external power supply.

microprocessor unit for temperature sensing, with less than ±0.5°C accuracy. This sensor can measure temperatures ranging from −55°C to +125°C. Unlike most of these sensors in the market, it also facilitates simple interfacing, programmable resolution from 9 bits to 12 bits with no external components required. Figure 11 shows the connection diagram of the temperature sensor and the microprocessor. This temperature sensor is decoupled using Kapton tape from the environment and fitted on the SPV module's backside. The relative module temperature is recorded while doing $I - V$ tracing using a microprocessor.

FIGURE 12. Pinout of SP-110-SS light irradiance sensor.

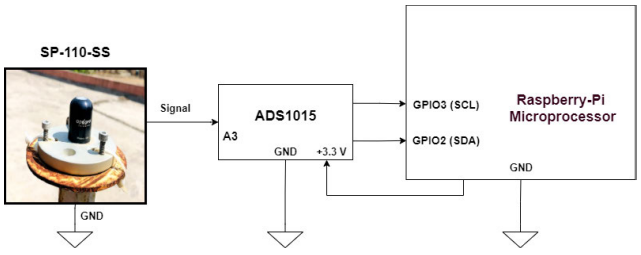

FIGURE 13. SP-110-SS light irradiance sensor connection diagram.

2) IRRADIATION MEASURING

The Apogee Instruments pyranometer SP-110-SS is used and installed as per the manufacture installation guidelines to measure solar light irradiance on the SPV module during the $I - V$ curve trace as shown in Figures 12, 13. This sensor is self-powered and has a spectral range of 360 to 1120 nm with a response time of 1 msec. To obtain correct readings, the manufacturer's method and components are used when mounting the pyranometer SP-SS-110. To improve precision, the sensor is positioned such that obstructions such as trees, objects, buildings, or other instruments do not shade it. The incident light radiation on a planar surface (which does not have to be horizontal), where the radiation emanates from all angles of a hemisphere, is directly proportional to the pyranometer sensor's output analog voltage signal. The sensor is leveled with an AL-100 leveling plate and fixed to a solid surface with nylon mounting screws to measure Photosynthetic Photon Flux Density (PPFD) incident on the horizontal plane surface. Azimuth error is usually less than one percent, and it is conveniently reduced by mounting the sensor with the cable pointed toward the true north in the northern hemisphere or south in the southern hemisphere. When not in use, the sensor top is covered by a protective covering cap supplied by the manufacturer.

3) VOLTAGE AND CURRENT MEASURING

The terminal current is measured using an ACS712 DC current sensor with a resolution of 0.1 A, a sensitivity of 100 mV/A, and an accuracy of 1%. It has three variants, out of which as per current ratings of the SPV module, here ACS712-20A variant is used. A highly accurate Digital Multimeter (DMM) with high voltage measuring capability is usually used to measure the output DC voltage of an SPV module. However, in this study, a simple resistor-based divider circuit is used with an external Analog to Digital Converter (ADC) for better data point resolution. A voltage divider is used to move down the DC output voltage to below 5 V using a combination of less tolerant 1 and 10 kW metal film resistors. The ADS1015, an external 12-bit analog to digital converter, converts the analog DC voltage to a digital value. Using a Raspberry Pi 3B, this digital value is then automatically logged for further processing.

D. CENTRAL PROCESSING UNIT (CPU)

In this study, the analog output of the SP-110-SS pyranometer is provided directly to the external four-channel ADC, which converts it to a digital equivalent value. If the light irradiance is greater than 700 W/m^2, the instantaneous analog output values of the voltage divider circuit and the ACS712 current sensor module are logged with the external ADC and the Raspberry pi. Simultaneously, the DB18B20 temperature sensor's output is logged directly by connecting the DS18B20 to the Raspberry pi GPIO4 pin. The Raspberry Pi 3B microprocessor, which is programmed with a Python script, first logs the data for future monitoring and processes it.

Python scripts record 750 data points for each current and voltage. It eliminates redundant points and plots $I - V$ and $P - V$ curves during processing. If the curve is multi-modal, the Python script starts retracing it. In this study, measurements were taken and provided under clear sky conditions, and all of this was handled by specially created Python scripts. The 7'inch touch screen display shows the $I-V$ curve from the data obtained during the sweep. To improve user interaction, IVCT is also programmed with a user-friendly Graphical User Interface (GUI) designed using a Python script. The logged real-time data of electrical and meteorological parameters are used for STC correction. The Wi-Fi and Ethernet modules built into the Raspberry Pi 3B model link IVCT to the network, allowing data to be transmitted wirelessly through the cloud or an IoT platform.

1) STC CORRECTION

This study has collected SPV performance data sets for accurate outdoor characterization. All SPV module manufacturers tests modules in laboratories under STC where light irradiance is 1000 W/m^2, module temperature is 25 °C, and reference solar spectral irradiance, i.e., the Air mass is 1.5, is maintained. These measurements are labeled at the SPV module's back site and provided in the datasheet as an SPV module reference specification [118]. However, these modules are mounted and used for power generation outdoor during their lifetime. Dependence of voltage and current measurement on sunlight intensity (G) and temperature of the module (T_m) can be normalized and estimated using equations 2, 3 [97]. The voltage temperature coefficient characterizes the open circuit voltage's strong dependence on SPV module temperature, while the influences due to light intensity is slight and follows a logarithmic function.

$$I_{STC} = [I_{meas}] * \left[\frac{G_{STC}}{G_{meas}}\right] * [1 - \alpha * (T_m - T_{STC})] \quad (2)$$

$$V_{STC} = \left[V_{meas} - V_T \ln\left(\frac{G_{meas}}{G_{STC}}\right)\right] * [1 - \beta * (T_m - T_{STC})] \quad (3)$$

where: I_{meas} and V_{meas} are the logged values of the current and voltage, respectively T_m is the measure module temperature using DS18B20 sensor, I_{STC} and V_{STC} are the values after irradiance correction, T_{STC} is the temperature at STC (25 °C), α and β are the current and voltage temperature correction coefficients of the SPV module used for the experiment which is given in datasheets. V_T is the module thermal voltage which can be calculated from equation 4 based on the ideal-diode model that omits series and shunt resistances.

$$V_T = \left[\frac{V_{oc,STC}}{\ln(I_{sc,STC}/I_o)}\right] * \left[\frac{T_m}{T_{STC}}\right] \quad (4)$$

where: $V_{oc,STC}$ and $I_{sc,STC}$ are the open circuit voltage and Short circuit current of the used SPV module at STC, I_o is the dark saturation current of the diode.

IV. EXPERIMENTAL RESULTS AND ANALYSIS

A. OUTCOMES OF RESISTIVE LOAD APPROACH

The findings obtained using the most commonly used traditional method for the 520 W_p power-rated SPV module are discussed in this section. These results would also assist in the validation of the proposed IVCT device's performance. As a resistive load, a 300 Ω rheostat is used with a slider that is manually shifted from the lowest resistance position to the highest resistance position. This method is simple, inexpensive, and yields valuable results for characterizing low-power SPV modules. The sampling frequency is determined by the operator's previous experience with the overall process. Table 4 shows the SPV module's electrical parameters extracted from sweeping $I - V$ and $P - V$ curves for the 520 W_p SPV module and associated meteorological parameters at different time instants on the same day using resistive load. However, based on the findings tabulated, it can be inferred that this method has certain disadvantages, such as low accuracy and inability to track continuously changing working and environmental circumstances. This method illustrates the inherent losses for high-power SPV modules due to heat dissipation during the operation.

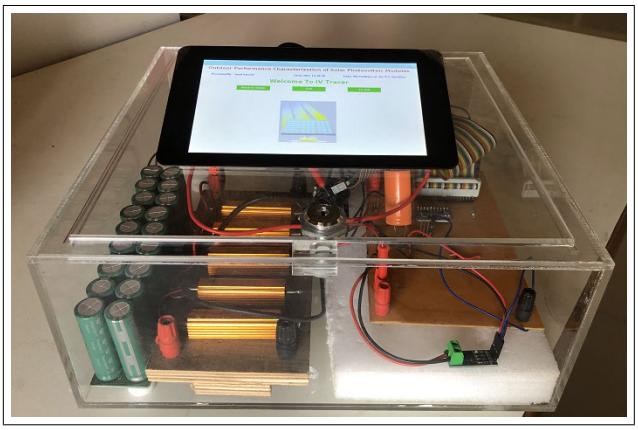

FIGURE 14. Proposed IVCT actual hardware setup.

B. OUTCOMES OF THE CAPACITIVE LOAD APPROACH

Figure 14 illustrates the proposed IVCT real hardware configuration. The SPV module's STC rating is used as a reference in error estimation and percent accuracy estimates. In this study, two modules of 260 W_p each are mounted on an outdoor location without nearby shading objects with the tilt angle of 18°. The SPV module's open-circuit voltage is the maximum DC output voltage between the two terminals of the SPV module. For safety and accuracy, the capacitor load's voltage rating should be greater than the V_{oc} value of the SPV module. The time required to sweep the characteristic curve is also affected by the capacitance of the load. 5.5 F 48.6 V supercapacitor load was chosen experimentally based on these selection criteria to optimize the proposed IVCT output and efficiency. The Scan Time (T_{scan}) needed to sweep the curve from I_{sc} to V_{oc} is calculated by the capacitance value used as a load, I_{sc}, and V_{oc} of the SPV module. In [107], the author proposed calculating T_{scan} in equation 5 by simplifying the voltage equations around the capacitive load while taking the Unity Fill Factor into account (UFF). In [119], the author further researched and proposed equation 6 to estimate T_{scan} for the SPV string level arrangement. The greater the capacitance value, the greater the (T_{scan}) needed to sweep the characteristic curve. These equations shows the relationship between T_{scan}, I_{sc}, V_{oc} and C. In this analysis, the SPS of an external ADC is calculated based on the estimated value of T_{scan}, known as the ADC Data Acquisition (DAQ) time. The ON period of switch S1 is predicted using T_{scan} and DAQ period, and this value is used during Python script programming. The T_{scan} calculations, chosen sampling frequency of ADC and the DAQ time calculation is summarized in Table 5.

$$T_{scan} = C * [V_{oc}/I_{sc}] \quad (5)$$

$$T_{scan} = 1.1 * C * [V_{oc}/I_{sc}] \quad (6)$$

TABLE 4. Outcomes of resistive load based IVCT for 520 W_p SPV module on the different time and respective Irradiance levels with result analysis.

$G\,(W/m^2)$	T_m (°C)		V_{oc}	V_m	I_{sc}	I_m	P_m
1000	25	Reference (A)	37.7	30.9	17.78	16.84	520.36
851	46	Measured	33.79	27.7	13.56	12.05	333.79
		STC Corrected (B)	36.55	30.06	15.8	14.04	422.04
		Absolute Error $[C = \|(A - B)\|]$	1.15	0.84	1.98	2.8	98.32
		Relative Error $[R_E = C/A]$	0.031	0.027	0.111	0.166	0.189
		% Accuracy $[\%D = 100 - \%R_E]$	96.9	97.3	88.9	83.4	81.1
902	49	Measured	33.71	27.62	13.78	12.18	336.41
		STC Corrected (B)	36.58	30.03	15.13	13.37	401.5
		Absolute Error $[C = \|(A - B)\|]$	1.12	0.87	2.65	3.47	118.86
		Relative Error $[R_E = C/A]$	0.03	0.028	0.149	0.206	0.228
		% Accuracy $[\%D = 100 - \%R_E]$	97	97.2	85.1	79.4	77.2
928	53	Measured	33.59	27.55	13.81	12.49	344.1
		STC Corrected (B)	36.77	30.2	14.71	13.31	401.96
		Absolute Error $[C = \|(A - B)\|]$	0.93	0.7	3.07	3.53	118.4
		Relative Error $[R_E = C/A]$	0.025	0.023	0.173	0.21	0.228
		% Accuracy $[\%D = 100 - \%R_E]$	97.5	97.7	82.7	79	77.2
947	55	Measured	33.53	27.49	14.08	12.98	356.82
		STC Corrected (B)	36.84	30.24	14.69	13.54	409.45
		Absolute Error $[C = \|(A - B)\|]$	0.86	0.66	3.09	3.3	110.91
		Relative Error $[R_E = C/A]$	0.023	0.021	0.174	0.196	0.213
		% Accuracy $[\%D = 100 - \%R_E]$	97.7	97.9	82.6	80.4	78.7
1021	59	Measured	33.45	27.51	14.58	13.42	369.18
		STC Corrected (B)	36.9	30.33	14.08	12.96	393.08
		Absolute Error $[C = \|(A - B)\|]$	0.8	0.57	3.7	3.88	127.28
		Relative Error $[R_E = C/A]$	0.021	0.018	0.208	0.23	0.245
		% Accuracy $[\%D = 100 - \%R_E]$	97.9	98.2	79.2	77	75.5

TABLE 5. The scan time calculation for the proposed IVCT device.

T_{scan} calculations for programming	
Data Rate of external ADC (ADS1015)	128 SPS
Data points of Current and Voltage	750 points each
Total sample data points	1500 points
Estimated scan time for external ADC	11.718 sec
Super Capacitor used in IVCT	5.5 F, 48.6 V
V_{oc} of the SPV module	37.7 V
I_{sc} of the SPV module	17.78 A
Estimated scan time using equation [5]	11.662 sec
Estimated scan time using equation [6]	12.828 sec
Measured scan time of proposed IVCT	14.3267 sec

All the instantaneous current and voltage data points are logged along with the module temperature and light irradiance at that timestamp. Table 6 summarizes the electrical parameters measured at ambient temperature and the corresponding STC converted data points, as well as the absolute error and measurement accuracy. Figures 15, 16 show the $I - V$ and $P - V$ characteristics of the SPV module taken on the same day at different time stamps using the proposed IVCT device. Each plot has 1500 data points with 14.3267sec scan time using the proposed IVCT. After all data points have been registered, the voltage and current values are STC converted using Eqs. 2, 3.

The proposed IVCT device has been tested in both uniform and non-uniform outdoor environmental conditions.

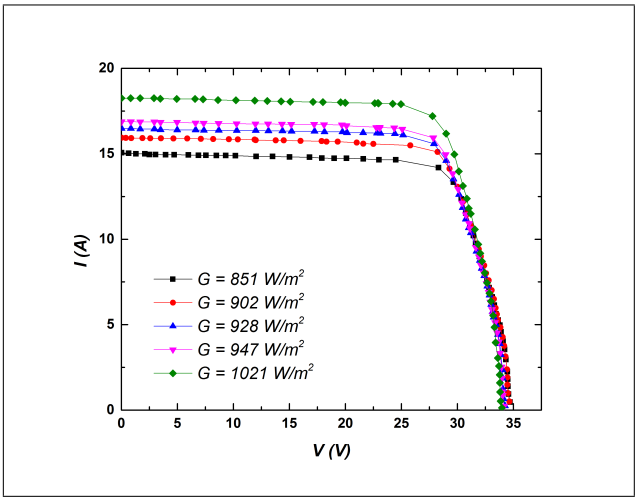

FIGURE 15. Captured $I - V$ plots using proposed IVCT for the different light radiance.

The Raspberry Pi 3B model used for Data Acquisition (DAQ), curve plotting, and computations have Wi-Fi and LAN networking built-in and can be easily connected to the network. The use of a 7' inch Raspberry Pi touch screen allows for onsite device inspections in remote areas where Wi-Fi or LAN network access is difficult to establish. It also has IoT

TABLE 6. Outcomes of capacitive load based IVCT for 520 W_p SPV module on the different time and respective irradiance levels with result analysis.

$G\ (W/m^2)$	T_m (°C)		V_{oc}	V_m	I_{sc}	I_m	P_m
1000	25	Reference (A)	37.7	30.9	17.78	16.84	520.356
851	46	Actual	34.69	28.32	15.06	14.19	401.86
		STC Corrected (B)	37.51	30.72	17.55	16.53	507.8
		Absolute Error $[C = \|(A - B)\|]$	0.19	0.18	0.23	0.31	12.56
		Relative Error $[R_E = C/A]$	0.005	0.006	0.013	0.018	0.024
		% Accuracy $[\%D = 100 - \%R_E]$	99.5	99.4	98.7	98.2	97.6
902	49	Actual	34.65	28.23	15.94	15.11	426.56
		STC Corrected (B)	37.59	30.69	17.5	16.59	509.15
		Absolute Error $[C = \|(A - B)\|]$	0.11	0.21	0.28	0.25	11.21
		Relative Error $[R_E = C/A]$	0.003	0.007	0.016	0.015	0.022
		% Accuracy $[\%D = 100 - \%R_E]$	99.7	99.3	98.4	98.5	97.8
928	53	Actual	34.24	27.91	16.49	15.59	435.12
		STC Corrected (B)	37.48	30.6	17.57	16.61	508.27
		Absolute Error $[C = \|(A - B)\|]$	0.22	0.3	0.21	0.23	12.09
		Relative Error $[R_E = C/A]$	0.006	0.01	0.012	0.014	0.023
		% Accuracy $[\%D = 100 - \%R_E]$	99.4	99	98.8	98.6	97.7
947	55	Actual	34.16	27.84	16.88	15.94	443.77
		STC Corrected (B)	37.53	30.62	17.61	16.63	509.21
		Absolute Error $[C = \|(A - B)\|]$	0.17	0.28	0.17	0.21	11.15
		Relative Error $[R_E = C/A]$	0.005	0.009	0.01	0.012	0.021
		% Accuracy $[\%D = 100 - \%R_E]$	99.5	99.1	99	98.8	97.9
1021	59	Actual	33.98	27.78	18.26	17.21	478.09
		STC Corrected (B)	37.49	30.63	17.64	16.63	509.38
		Absolute Error $[C = \|(A - B)\|]$	0.21	0.27	0.14	0.21	10.98
		Relative Error $[R_E = C/A]$	0.006	0.009	0.008	0.012	0.021
		% Accuracy $[\%D = 100 - \%R_E]$	99.4	99.1	99.2	98.8	97.9

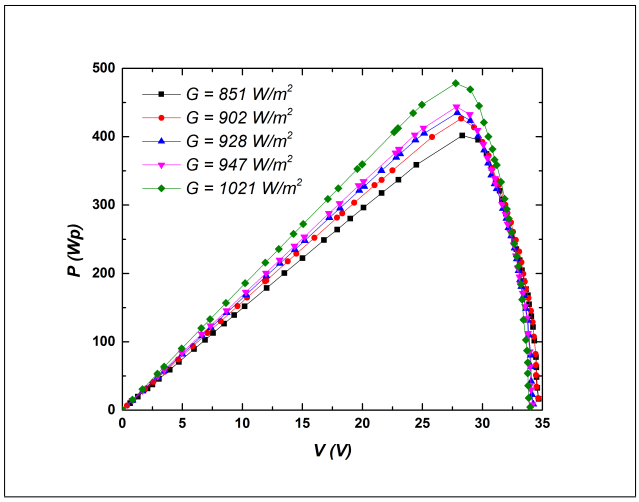

FIGURE 16. Captured $P - V$ plots using proposed IVCT for the different light radiance.

capabilities, as the collected data sets are sent to the ThingSpeak IoT Remote Access Portal (RAP) for further processing and review of the recorded I–V and P–V curves. It will improve the hardware's efficiency and stability. Collected real-time data can be processed and measured at any time and from any place to take the appropriate measures to preserve the SPV module's performance. A user-friendly GUI is created using Python libraries to view $I - V$ and $P - V$ curves locally for better conceptual understanding. This proposed IVCT device aids the service engineer in detecting early-stage faults and scheduling maintenance accordingly, which also aids in predicting power plant deterioration.

C. SUMMARY

The resistive load approach obtained 98.2 percent accuracy for voltage measurement on a 520 *Wp* SPV module, while the capacitive load method manages 99.7 percent accuracy after STC conversion. Similarly, resistive load and capacitive load give a percentage accuracy of 88.9 and 99.2 percent, respectively, for current measurements. The current measurement precision shows the minimal impact of change in irradiance while tracing curves using the proposed IVCT, which is also visible by accuracy calculations for measuring current. This result demonstrates that capacitors can measure characteristic curves under uniform and changing environmental conditions and provide reliable and accurate results when used as the load. Using a capacitor-based load approach while designing IVCT will increase the feasibility and robustness of the design setup under non-uniform conditions.

Considering the highest light radiance level of 1021 W/m^2, the resistive load's percentage accuracy for the maximum

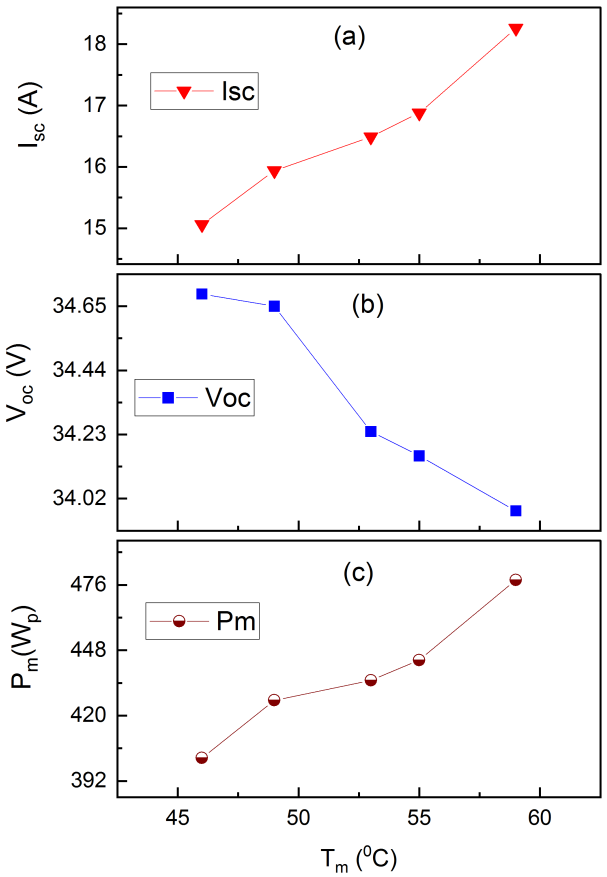

FIGURE 17. I_{sc}, V_{oc} and P_{max} as a function of T_m.

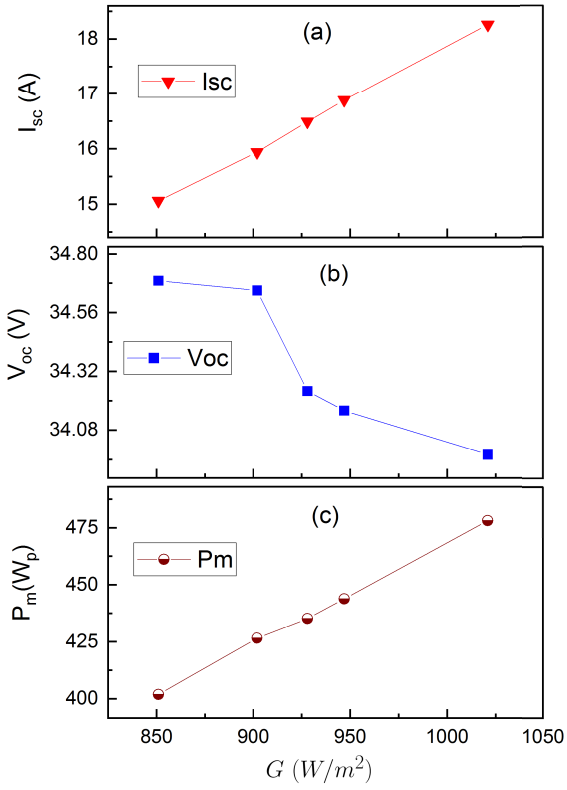

FIGURE 18. I_{sc}, V_{oc} and P_{max} as a function of G.

power measurement is 75.5 percentage while the capacitive load is 97.9 percentage. More current will flow for high irradiance intensity, resulting in high output power, which resembles the capacitive load-based approach. It shows that the capacitive load method is more reliable, robust, faithful, and accurate than the resistive load. Figures 18, 17 illustrates the influence of G and Tm on the measurement of instantaneous voltage, current, and power data points. Figure 18 reveals that the logged current value is smaller at a light irradiance of 851 $W/m2$ than at a light irradiance of 1021 $W/m2$. It shows that the greater the light irradiance, the higher the current, but the voltage just marginally decreases as the module temperature rises. The voltage and current data points calculated by the IVCT show a maximum at G of 1021 $W/m2$.

The on-field characterization of a solar cell or module is helpful since it is vulnerable to many module design issues such as spectral response, interconnection issues, optical alignment effects, thermal control issues, bypass diode faults, and parasitic impedances. The analysis of extracted device parameters gives valuable information to identify the possible SPV array anomalies like hot spot, loose connection, broken cell, etc. The error during measurements is also due to the manufacturing losses [120], [121]. Following are the reasons for I–V curve shape variation for impairment, which can also be used to analyze the $I - V$ curve and draw conclusions based on the same shape. These methods were designed to bring together the best practices and years of experience in the field of SPV degradation analysis.

1) Incompatibility between SPV modules or SPV arrays leads to steps or notches in the $I-V$ curve shape. These are most often affected by shading and soiling caused by a tree branch, a structure, or dust that obscures a portion of the solar panels, allowing solar radiation to be unevenly distributed among the SPV modules [122].
2) A rounder knee is a result of the aging process.
3) A low output current of the SPV module signifies uniform degradation, fading, or soiling.
4) The SPV module's low output voltage indicates that the bypass diodes have been shorted or that Potential-Induced Degradation (PID) has occurred.
5) A shallower slope in the voltage source area (From (V_m, I_m) to (V_{oc},0)) suggests an increase in the SPV module's series resistance or wire defects.
6) A steeper slope in the current source region due to SPV module mismatches or the SPV cells' shunt paths.

V. CONCLUSION

In this study, a novel IVCT design is proposed for accurately and successfully characterizing high power-rated SPV modules' actual operating status. The IVCT device circuit prototype has been designed and tested. It also includes low-power light irradiance and temperature sensors to collect data on essential environmental conditions, as well as Python-based tools for data management, storage, plotting, and querying.

To rapidly sweep the output $I-V$ characteristic curves of SPV modules, the IVCT primarily utilizes the capacitor charging path. To obtain a consistent sampling of the entire $I-V$ curve, we propose an adaptive sampling interval for high-resolution characteristic curves and charging and discharging time estimation methods. The time it takes to measure the entire $I-V$ curve is usually calculated in few seconds, depending on the capacitor's value. The IVCT device can quickly obtain a high-quality and complete characteristic curve for high-power rating SPV modules based on field test results. The proposed IVCT can be used to measure high power rated SPV modules with I_{sc} of up to 20 A and an V_{oc} of up to 45 V, depending on the primary component rating performance. Finally, a summary of the causes of characterization curve shape variance for impairment which can also be used to analyze the $I-V$ curve and draw conclusions based on the shape of the same has been presented. The losses and measurement error are primarily due to the power losses caused by the SPV module's intrinsic function, known as degradation losses, and the losses caused by not being at the optimum operating point, known as mismatch losses.

VI. FUTURE SCOPE

Extending IVCT design methodology to characterize higher power rated SPV module and arrays, the effect of scalability on the performance of electronic components, and the measurement accuracy is taken up as future work. The use of artificial intelligence algorithms to predict SPV health and its causes by analyzing the shape of captured $I-V$ characteristic curves can be seen as future work.

REFERENCES

[1] H. E. Murdock, D. Gibb, T. André, J. L. Sawin, A. Brown, F. Appavou, G. Ellis, B. Epp, F. Guerra, and F. Joubert, "Renewables 2020-global status report," Global Trends Renew. Energy Investment, Frankfurt School-UNEP Collaborating Centre Climate Sustain. Energy Finance, BloombergNEF, UN Environ. Programme, Paris, France, Tech. Rep. REN21, 2020. [Online]. Available: https://www.ren21.net/wp-content/uploads/2019/05/gsr_2020_full_report_en.pdf

[2] G. P. Peters, R. M. Andrew, J. G. Canadell, P. Friedlingstein, R. B. Jackson, J. I. Korsbakken, C. Le Quéré, and A. Peregon, "Carbon dioxide emissions continue to grow amidst slowly emerging climate policies," *Nature Climate Change*, vol. 10, no. 1, pp. 3–6, Jan. 2020.

[3] J. G. J. Olivier and J. A. H. W. Peters, "Trends in global Co_2 and total greenhouse gas emissions: 2020 report," in *PBL Netherlands Environment*. The Hague, The Netherlands: Assessment Agency, 2020.

[4] M. A. Aktar, M. M. Alam, and A. Q. Al-Amin, "Global economic crisis, energy use, CO_2 emissions, and policy roadmap amid COVID-19," *Sustain. Prod. Consumption*, vol. 26, pp. 770–781, Apr. 2021.

[5] J. Sayyad and P. Nasikkar, "Solar photovoltaic performance monitoring: A bibliometric review, research gaps and opportunities," *Library Philosophy Pract. (e-J.)*, pp. 1–25, Dec. 2020. [Online]. Available: https://digitalcommons.unl.edu/libphilprac/4830/

[6] C. Reise, B. Müller, D. Moser, G. Belluardo, and P. Ingenhoven, "Uncertainties in PV system yield predictions and assessments," Int. Energy Agency, Paris, France, Tech. Rep. IEA-PVPS T13-12, 2018. [Online]. Available: https://iea-pvps.org/wp-content/uploads/2020/01/Uncertainties_in_PV_System_Yield_Predictions_and_Assessments_by_Task_13.pdf

[7] R. Srivastava, A. N. Tiwari, and V. K. Giri, "An overview on performance of PV plants commissioned at different places in the world," *Energy Sustain. Develop.*, vol. 54, pp. 51–59, Feb. 2020.

[8] *Future of Solar Photovoltaic: Deployment, Investment, Technology, Grid Integration, and Socio-Economic Aspects*, IRENA, Abu Dhabi, United Arab Emirates, 2019.

[9] B. Shiva Kumar and K. Sudhakar, "Performance evaluation of 10 MW grid connected solar photovoltaic power plant in India," *Energy Rep.*, vol. 1, pp. 184–192, Nov. 2015.

[10] C. Huang and L. Wang, "Simulation study on the degradation process of photovoltaic modules," *Energy Convers. Manage.*, vol. 165, pp. 236–243, Jun. 2018.

[11] H. I. Dag and M. S. Buker, "Performance evaluation and degradation assessment of crystalline silicon based photovoltaic rooftop technologies under outdoor conditions," *Renew. Energy*, vol. 156, pp. 1292–1300, Aug. 2020.

[12] J. E. F. da Fonseca, F. S. de Oliveira, C. W. Massen Prieb, and A. Krenzinger, "Degradation analysis of a photovoltaic generator after operating for 15 years in Southern Brazil," *Sol. Energy*, vol. 196, pp. 196–206, Jan. 2020.

[13] D. C. Jordan, T. J. Silverman, B. Sekulic, and S. R. Kurtz, "PV degradation curves: Non-linearities and failure modes," *Prog. Photovolt., Res. Appl.*, vol. 25, no. 7, pp. 583–591, Jul. 2017.

[14] J.-A. Jiang, J.-C. Wang, K.-C. Kuo, Y.-L. Su, and J.-C. Shieh, "On evaluating the effects of the incident angle on the energy harvesting performance and MPP estimation of PV modules," *Int. J. Energy Res.*, vol. 38, no. 10, pp. 1304–1317, Aug. 2014.

[15] J. K. Sayyad and P. S. Nasikkar, "Solar photovoltaic module performance characterisation using single diode modeling," in *Proc. E3S Web Conf.*, vol. 170, 2020, Art. no. 01023.

[16] G. Rediske, J. C. M. Siluk, N. G. Gastaldo, P. D. Rigo, and C. B. Rosa, "Determinant factors in site selection for photovoltaic projects: A systematic review," *Int. J. Energy Res.*, vol. 43, no. 5, pp. 1689–1701, Apr. 2019.

[17] D. C. Jordan, S. R. Kurtz, K. VanSant, and J. Newmiller, "Compendium of photovoltaic degradation rates," *Prog. Photovolt., Res. Appl.*, vol. 24, no. 7, pp. 978–989, Jul. 2016.

[18] F. Obeidat, "A comprehensive review of future photovoltaic systems," *Sol. Energy*, vol. 163, pp. 545–551, Mar. 2018.

[19] M. B. Hayat, D. Ali, K. C. Monyake, L. Alagha, and N. Ahmed, "Solar energy–A look into power generation, challenges, and a solar-powered future," *Int. J. Energy Res.*, vol. 43, no. 3, pp. 1049–1067, Mar. 2019.

[20] M. S. Ismail, M. Moghavvemi, and T. M. I. Mahlia, "Characterization of PV panel and global optimization of its model parameters using genetic algorithm," *Energy Convers. Manage.*, vol. 73, pp. 10–25, Sep. 2013.

[21] E. Karatepe, M. Boztepe, and M. Colak, "Neural network based solar cell model," *Energy Convers. Manage.*, vol. 47, nos. 9–10, pp. 1159–1178, Jun. 2006.

[22] F. Ghani, G. Rosengarten, M. Duke, and J. K. Carson, "On the influence of temperature on crystalline silicon solar cell characterisation parameters," *Sol. Energy*, vol. 112, pp. 437–445, Feb. 2015.

[23] F. Khan, S.-H. Baek, Y. Park, and J. H. Kim, "Extraction of diode parameters of silicon solar cells under high illumination conditions," *Energy Convers. Manage.*, vol. 76, pp. 421–429, Dec. 2013.

[24] A. Bouraiou, M. Hamouda, A. Chaker, M. Mostefaoui, S. Lachtar, M. Sadok, N. Boutasseta, M. Othmani, and A. Issam, "Analysis and evaluation of the impact of climatic conditions on the photovoltaic modules performance in the desert environment," *Energy Convers. Manage.*, vol. 106, pp. 1345–1355, Dec. 2015.

[25] P. Dash and N. Gupta, "Effect of temperature on power output from different commercially available photovoltaic modules," *Int. J. Eng. Res. Appl.*, vol. 5, no. 1, pp. 148–151, 2015.

[26] C. Riley and L. Tolbert, "An online autonomous I–V tracer for PV monitoring applications," in *Proc. IEEE Power Energy Soc. Gen. Meeting*, Jul. 2015, pp. 1–5.

[27] Z. Chen, Y. Chen, L. Wu, S. Cheng, and P. Lin, "Deep residual network based fault detection and diagnosis of photovoltaic arrays using current-voltage curves and ambient conditions," *Energy Convers. Manage.*, vol. 198, Oct. 2019, Art. no. 111793.

[28] Y. Hishikawa, T. Doi, M. Higa, K. Yamagoe, and H. Ohshima, "Precise outdoor PV module performance characterization under unstable irradiance," *IEEE J. Photovolt.*, vol. 6, no. 5, pp. 1221–1227, Sep. 2016.

[29] J.-M. Huang, R.-J. Wai, and W. Gao, "Newly-designed fault diagnostic method for solar photovoltaic generation system based on IV-curve measurement," *IEEE Access*, vol. 7, pp. 70919–70932, 2019.

[30] N. Umachandran and G. TamizhMani, "Effect of spatial temperature uniformity on outdoor photovoltaic module performance characterization," in *Proc. IEEE 43rd Photovoltaic Spec. Conf. (PVSC)*, Jun. 2016, pp. 2731–2737.

[31] M. Dhimish and Z. Chen, "Novel open-circuit photovoltaic bypass diode fault detection algorithm," *IEEE J. Photovolt.*, vol. 9, no. 6, pp. 1819–1827, Nov. 2019.
[32] I. R. Balasubramanian, S. Ilango Ganesan, and N. Chilakapati, "Impact of partial shading on the output power of PV systems under partial shading conditions," *IET Power Electron.*, vol. 7, no. 3, pp. 657–666, Mar. 2014.
[33] M. Dhimish, V. Holmes, B. Mehrdadi, M. Dales, B. Chong, and L. Zhang, "Seven indicators variations for multiple PV array configurations under partial shading and faulty PV conditions," *Renew. Energy*, vol. 113, pp. 438–460, Dec. 2017.
[34] A. Haque, K. V. S. Bharath, M. A. Khan, I. Khan, and Z. A. Jaffery, "Fault diagnosis of photovoltaic modules," *Energy Sci. Eng.*, vol. 7, no. 3, pp. 622–644, Jun. 2019.
[35] J. E. Quiroz, J. S. Stein, C. K. Carmignani, and K. Gillispie, "*In-situ* module-level I–V tracers for novel PV monitoring," in *Proc. IEEE 42nd Photovoltaic Spec. Conf. (PVSC)*, Jun. 2015, pp. 1–6.
[36] X. Ma, W.-H. Huang, E. Schnabel, M. Köhl, J. Brynjarsdóttir, J. L. Braid, and R. H. French, "Data-driven $I--V$ feature extraction for photovoltaic modules," *IEEE J. Photovolt.*, vol. 9, no. 5, pp. 1405–1412, Sep. 2019.
[37] M. D. Yandt, J. P. Cook, M. Kelly, H. Schriemer, and K. Hinzer, "Dynamic real-time $I - -V$ curve measurement system for indoor/outdoor characterization of photovoltaic cells and modules," *IEEE J. Photovolt.*, vol. 5, no. 1, pp. 337–343, Jan. 2015.
[38] C. B. Jones, M. Martinez-Ramon, R. Smith, C. K. Carmignani, O. Lavrova, C. Robinson, and J. S. Stein, "Automatic fault classification of photovoltaic strings based on an *in situ* IV characterization system and a Gaussian process algorithm," in *Proc. IEEE 43rd Photovoltaic Specialists Conf. (PVSC)*, Jun. 2016, pp. 1708–1713.
[39] Z. Chen, L. Wu, S. Cheng, P. Lin, Y. Wu, and W. Lin, "Intelligent fault diagnosis of photovoltaic arrays based on optimized kernel extreme learning machine and I-V characteristics," *Appl. Energy*, vol. 204, pp. 912–931, Oct. 2017.
[40] A. A. K. Ismaeel, E. H. Houssein, D. Oliva, and M. Said, "Gradient-based optimizer for parameter extraction in photovoltaic models," *IEEE Access*, vol. 9, pp. 13403–13416, 2021.
[41] A. A. Z. Diab, H. M. Sultan, R. Aljendy, A. S. Al-Sumaiti, M. Shoyama, and Z. M. Ali, "Tree growth based optimization algorithm for parameter extraction of different models of photovoltaic cells and modules," *IEEE Access*, vol. 8, pp. 119668–119687, 2020.
[42] C. W. Hansen and B. H. King, "Determining series resistance for equivalent circuit models of a PV module," *IEEE J. Photovolt.*, vol. 9, no. 2, pp. 538–543, Mar. 2019.
[43] R. Ahmad, A. F. Murtaza, U. T. Shami, Zulqarnain, and F. Spertino, "An MPPT technique for unshaded/shaded photovoltaic array based on transient evolution of series capacitor," *Sol. Energy*, vol. 157, pp. 377–389, Nov. 2017.
[44] E. Kandemir, N. S. Cetin, and S. Borekci, "A comprehensive overview of maximum power extraction methods for PV systems," *Renew. Sustain. Energy Rev.*, vol. 78, pp. 93–112, Oct. 2017.
[45] A. Ghosh, "Soiling losses: A barrier for India's energy security dependency from photovoltaic power," *Challenges*, vol. 11, no. 1, p. 9, 2020.
[46] M. R. Maghami, H. Hizam, C. Gomes, M. A. Radzi, M. I. Rezadad, and S. Hajighorbani, "Power loss due to soiling on solar panel: A review," *Renew. Sustain. Energy Rev.*, vol. 59, pp. 1307–1316, Jun. 2016.
[47] J. R. Caron and B. Littmann, "Direct monitoring of energy lost due to soiling on first solar modules in California," *IEEE J. Photovolt.*, vol. 3, no. 1, pp. 336–340, Jan. 2013.
[48] L. G. Monteiro, W. N. Macedo, R. L. Cavalcante, W. B. Junior, P. F. Torres, T. R. Brito, M. M. Silva, B. M. Lopes, J. M. Fraga, D. D. Alves, O. A. Chase, and W. C. Boaventura, "Field I-V curve measurements methodology at string level to monitor failures and the degradation process: A case study of a 1.42 MWp PV power plant," *IEEE Access*, vol. 8, pp. 226845–226865, 2020.
[49] A. Wang and Y. Xuan, "Close examination of localized hot spots within photovoltaic modules," *Energy Convers. Manage.*, vol. 234, Apr. 2021, Art. no. 113959.
[50] S. Tang, Y. Xing, L. Chen, X. Song, and F. Yao, "Review and a novel strategy for mitigating hot spot of PV panels," *Sol. Energy*, vol. 214, pp. 51–61, Jan. 2021.
[51] M. Dhimish, V. Holmes, P. Mather, and M. Sibley, "Novel hot spot mitigation technique to enhance photovoltaic solar panels output power performance," *Sol. Energy Mater. Sol. Cells*, vol. 179, pp. 72–79, Jun. 2018.
[52] Z. Chen, Y. Lin, L. Wu, S. Cheng, and P. Lin, "Development of a capacitor charging based quick I-V curve tracer with automatic parameter extraction for photovoltaic arrays," *Energy Convers. Manage.*, vol. 226, Dec. 2020, Art. no. 113521.
[53] J. Sayyad, P. Nasikkar, A. P. Singh, and S. Ozana, "Capacitive load-based smart OTF for high power rated SPV module," *Energies*, vol. 14, no. 3, p. 788, Feb. 2021.
[54] R. K. Pachauri, H. H. Alhelou, J. Bai, and M. E. H. Golshan, "Adaptive switch matrix for PV module connections to avoid permanent cross-tied link in PV array system under non-uniform irradiations," *IEEE Access*, vol. 9, pp. 45978–45992, 2021.
[55] A. Q. Malik and S. J. B. H. Damit, "Outdoor testing of single crystal silicon solar cells," *Renew. Energy*, vol. 28, no. 9, pp. 1433–1445, Jul. 2003.
[56] H. Amiry, M. Benhmida, R. Bendaoud, C. Hajjaj, S. Bounouar, S. Yadir, K. Raïs, and M. Sidki, "Design and implementation of a photovoltaic I-V curve tracer: Solar modules characterization under real operating conditions," *Energy Convers. Manage.*, vol. 169, pp. 206–216, Aug. 2018.
[57] A. Tihane, M. Boulaid, A. Ihlal, and M. Nya, "Design and implementation of a low cost automatic variable load and data acquisition for characterization of photovoltaic modules simultaneously," *Int. Rev. Autom. Control (IREACO)*, vol. 9, no. 1, p. 48, Jan. 2016.
[58] E. Durán, J. Andújar, J. Enrique, and J. Pérez-Oria, "Determination of PV generator IV/PV characteristic curves using a DC-DC converter controlled by a virtual instrument," *Int. J. Photoenergy*, vol. 2012, Jan. 2012, Art. no. 843185.
[59] P. Sanchis, J. Lopez, A. Ursua, and L. Marroyo, "Electronic controlled device for the analysis and design of photovoltaic systems," *IEEE Power Electron Lett.*, vol. 3, no. 2, pp. 57–62, Jun. 2005.
[60] S. Sarikh, M. Raoufi, A. Bennouna, A. Benlarabi, and B. Ikken, "Implementation of a plug and play I-V curve tracer dedicated to characterization and diagnosis of PV modules under real operating conditions," *Energy Convers. Manage.*, vol. 209, Apr. 2020, Art. no. 112613.
[61] P. Papageorgas, D. Piromalis, T. Valavanis, S. Kambasis, T. Iliopoulou, and G. Vokas, "A low-cost and fast PV I-V curve tracer based on an open source platform with M2M communication capabilities for preventive monitoring," *Energy Procedia*, vol. 74, pp. 423–438, Aug. 2015.
[62] T. Mambrini, "Characterization of photovoltaic solar panels in real conditions of implantation and according to different technologies," Ph.D. dissertation, Université Paris Sud-Paris XI, Paris, France, 2014. [Online]. Available: https://tel.archives-ouvertes.fr/tel-01164783/file/VD2_MAMBRINI_THOMAS_16122014.pdf
[63] Y. Kuai and S. Yuvarajan, "An electronic load for testing photovoltaic panels," *J. Power Sources*, vol. 154, no. 1, pp. 308–313, Mar. 2006.
[64] N. Forero, J. Hernández, and G. Gordillo, "Development of a monitoring system for a PV solar plant," *Energy Convers. Manage.*, vol. 47, nos. 15–16, pp. 2329–2336, Sep. 2006.
[65] M. Guvench, C. Gurcan, K. Durgin, and D. MacDonald, "Solar simulator and IV measurement system for large area solar cell testing," in *Proc. Amer. Soc. Eng. Educ. Annu. Conf. Expo.*, vol. 9, 2004, pp. 1–7.
[66] B.-C. Feng, J.-H. Su, W.-T. Liu, and C.-H. Peng, "Technology of photovoltaic array characteristic test based on variable electronic load," *Power Electron.*, vol. 45, no. 9, pp. 38–45, 2011.
[67] Y. Erkaya, I. Flory, and S. X. Marsillac, "Development of a string level I–V curve tracer," in *Proc. IEEE 40th Photovoltaic Spec. Conf. (PVSC)*, Jun. 2014, pp. 3104–3107.
[68] D. T. Cotfas, P. A. Cotfas, D. Ursutiu, and C. Samoila, "Current-voltage characteristic raising techniques for solar cells. Comparisons and applications," in *Proc. 12th Int. Conf. Optim. Electr. Electron. Equip.*, May 2010, pp. 1115–1120.
[69] J. Muñoz and E. Lorenzo, "Capacitive load based on IGBTs for on-site characterization of PV arrays," *Sol. Energy*, vol. 80, no. 11, pp. 1489–1497, Nov. 2006.
[70] F. Spertino, J. Ahmad, A. Ciocia, P. Di Leo, F. Ali Murtaza, and M. Chiaberge, "Capacitor charging method for $I - -V$ curve tracer and MPPT in photovoltaic systems," *Sol. Energy*, vol. 119, pp. 461–473, Sep. 2015.
[71] E. Ortega, G. Aranguren, and J. C. Jimeno, "New monitoring method to characterize individual modules in large photovoltaic systems," *Sol. Energy*, vol. 193, pp. 906–914, Nov. 2019.
[72] I. W. Reischauer and A. J. Rix, "Design of a low cost multi-module capacitive IV curve tracer for PV module mismatch characterisation," in *Proc. Southern Afr. Universities Power Eng. Conf./Robot. Mechatronics/Pattern Recognit. Assoc. South Afr. (SAUPEC/RobMech/PRASA)*, Jan. 2019, pp. 340–346.
[73] P. S. Nasikkar and J. K. Sayyad, "Internet of Things (IoT) based outdoor performance characterisation of solar photovoltaic module," in *Proc. E3S Web Conf.*, vol. 170, 2020, Art. no. 02009.

[74] H. Chi, M. Tajuddin, N. Ghazali, A. B. Azmi, and M. Maaz, "Internet of Things (IoT) based iv curve tracer for photovoltaic monitoring systems," *Indonesian J. Electr. Eng. Comput. Sci.*, vol. 13, no. 3, pp. 1022–1030, 2019.
[75] A. A. Willoughby, T. V. Omotosho, and A. P. Aizebeokhai, "A simple resistive load I-V curve tracer for monitoring photovoltaic module characteristics," in *Proc. 5th Int. Renew. Energy Congr. (IREC)*, Mar. 2014, pp. 1–6.
[76] A. Rivai and N. A. Rahim, "A low-cost photovoltaic (PV) array monitoring system," in *Proc. IEEE Conf. Clean Energy Technol. (CEAT)*, Nov. 2013, pp. 169–174.
[77] A. A. Willoughby and M. O. Osinowo, "Development of an electronic load I-V curve tracer to investigate the impact of harmattan aerosol loading on PV module pern2tkformance in Southwest Nigeria," *Sol. Energy*, vol. 166, pp. 171–180, May 2018.
[78] E. V. Dyk, A. Gxasheka, and E. Meyer, "Monitoring current–voltage characteristics and energy output of silicon photovoltaic modules," *Renew. Energy*, vol. 30, no. 3, pp. 399–411, 2005.
[79] E. E. van Dyk, A. R. Gxasheka, and E. L. Meyer, "Monitoring current-voltage characteristics of photovoltaic modules," in *Proc. Conf. Rec. 29th IEEE Photovoltaic Spec. Conf.*, May 2002, pp. 1516–1519.
[80] A. Rivai and N. A. Rahim, "Binary-based tracer of photovoltaic array characteristics," *IET Renew. Power Gener.*, vol. 8, no. 6, pp. 621–628, 2014.
[81] V. Leite, J. Batista, F. Chenlo, and J. L. Afonso, "Low-cost instrument for tracing I-V characteristics of photovoltaic modules," in *Proc. Int. Conf. Renew. Energies Power Qual. (ICREPQ)*, Santiago de Compostela, Spain, vol. 1, no. 10, Mar./Apr. 2012, pp. 1012–1017. [Online]. Available: http://www.icrepq.com/icrepq'12/565-leite.pdf
[82] V. Leite and F. Chenlo, "An improved electronic circuit for tracing the IV characteristics of photovoltaic modules and strings," in *Proc. Int. Conf. Renew. Energies Power Qual. (ICREPQ)*, vol. 1, no. 8, Apr. 2010, pp. 1224–1228. [Online]. Available: http://icrepq.com/icrepq'10/629-Leite.pdf
[83] R. E. Campos, E. Y. Sako, H. S. Moreira, J. L. de Souza Silva, and M. G. Villalva, "Experimental analysis of a developed I-V curve tracer under partially shading conditions," in *Proc. IEEE PES Innov. Smart Grid Technol. Conf.-Latin Amer. (ISGT Latin Amer.)*, Sep. 2019, pp. 1–5.
[84] C. Ranhotigamage and S. C. Mukhopadhyay, "Field trials and performance monitoring of distributed solar panels using a low-cost wireless sensors network for domestic applications," *IEEE Sensors J.*, vol. 11, no. 10, pp. 2583–2590, Oct. 2011.
[85] P. Papageorgas, D. Piromalis, K. Antonakoglou, G. Vokas, D. Tseles, and K. G. Arvanitis, "Smart solar panels: *In-situ* monitoring of photovoltaic panels based on wired and wireless sensor networks," *Energy Procedia*, vol. 36, pp. 535–545, 2013.
[86] A. Vega, V. Valiño, E. Conde, A. Ramos, and P. Reina, "Double sweep tracer for I-V curves characterization and continuous monitoring of photovoltaic facilities," *Sol. Energy*, vol. 190, pp. 622–629, Sep. 2019.
[87] V. Leite, J. Batista, F. Chenlo, and J. L. Afonso, "Low-cost I-V tracer for photovoltaic modules and strings," in *Proc. Int. Symp. Power Electron., Electr. Drives, Autom. Motion*, Jun. 2014, pp. 971–976.
[88] A. Sahbel, N. Hassan, M. M. Abdelhameed, and A. Zekry, "Experimental performance characterization of photovoltaic modules using DAQ," *Energy Procedia*, vol. 36, pp. 323–332, 2013.
[89] F. Spertino, J. Sumaili, H. Andrei, and G. Chicco, "PV module parameter characterization from the transient charge of an external capacitor," *IEEE J. Photovolt.*, vol. 3, no. 4, pp. 1325–1333, Oct. 2013.
[90] K. V. G. Raghavendra, K. Zeb, A. Muthusamy, T. Krishna, S. Kumar, D.-H. Kim, M.-S. Kim, H.-G. Cho, and H.-J. Kim, "A comprehensive review of DC–DC converter topologies and modulation strategies with recent advances in solar photovoltaic systems," *Electronics*, vol. 9, no. 1, p. 31, 2020.
[91] S. Singer, "The application of loss-free resistors in power processing circuits," *IEEE Trans. Power Electron.*, vol. 6, no. 4, pp. 595–600, Oct. 1991.
[92] I. F. Silva, P. S. Vicente, F. L. Tofoli, and E. M. Vicente, "Portable and low cost photovoltaic curve tracer," in *Proc. Brazilian Power Electron. Conf. (COBEP)*, Nov. 2017, pp. 1–6.
[93] M. Kazerani, "A high-performance controllable DC load," in *Proc. IEEE Int. Symp. Ind. Electron.*, Jun. 2007, pp. 1015–1020.
[94] T. A. Pereira, L. Schmitz, W. M. D. Santos, D. C. Martins, and R. F. Coelho, "Design of a portable photovoltaic $I--V$ curve tracer based on the DC–DC converter method," *IEEE J. Photovolt.*, vol. 11, no. 2, pp. 552–560, Mar. 2021.
[95] R. S. Ameen and R. S. Balog, "Flexible and scalable photovoltaic curve tracer," in *Proc. Int. Conf. Photovoltaic Sci. Technol. (PVCon)*, Jul. 2018, pp. 1–4.
[96] S. Gaiotto, A. Laudani, F. R. Fulginei, and A. Salvini, "An advanced measurement equipment for the tracing of photovoltaic panel I–V curves," in *Proc. Int. Conf. Renew. Energy Res. Appl. (ICRERA)*, Nov. 2015, pp. 1010–1014.
[97] Y. Erkaya, P. Moses, and S. Marsillac, "On-site characterization of PV modules using a portable, MOSFET-based capacitive load," in *Proc. IEEE 43rd Photovoltaic Spec. Conf. (PVSC)*, Jun. 2016, pp. 3119–3122.
[98] Q. Xiong, S. Ji, X. Liu, X. Feng, F. Zhang, L. Zhu, A. L. Gattozzi, and R. E. Hebner, "Detecting and localizing series arc fault in photovoltaic systems based on time and frequency characteristics of capacitor current," *Sol. Energy*, vol. 170, pp. 788–799, Aug. 2018.
[99] Z. Chen, W. Lin, L. Wu, C. Long, P. Lin, and S. Cheng, "A capacitor based fast I-V characteristics tester for photovoltaic arrays," *Energy Procedia*, vol. 145, pp. 381–387, Jul. 2018.
[100] H. M. Aguilar, R. F. Maldonado, and L. B. Navarro, "Charging a capacitor with a photovoltaic module," *Phys. Educ.*, vol. 52, no. 4, Jul. 2017, Art. no. 045016.
[101] F. Recart, H. Mackel, A. Cuevas, and R. A. Sinton, "Simple data acquisition of the current-voltage and illumination-voltage curves of solar Cells1," in *Proc. IEEE 4th World Conf. Photovoltaic Energy Conf.*, May 2006, pp. 1215–1218.
[102] M. Meiqin, S. Jianhui, L. Chang, P. Kai, Z. Guorong, and D. Ming, "Research and development of fast field tester for characteristics of solar array," in *Proc. Can. Conf. Electr. Comput. Eng.*, May 2009, pp. 1055–1060.
[103] E. Velilla, J. B. Cano, and F. Jaramillo, "Monitoring system to evaluate the outdoor performance of solar devices considering the power rating conditions," *Sol. Energy*, vol. 194, pp. 79–85, Dec. 2019.
[104] S. Basu Pal, A. Das, K. Das (Bhattacharya), and D. Mukherjee, "Design of a low-cost measuring and plotting device for photovoltaic modules," *Meas. Control*, vol. 52, nos. 9–10, pp. 1308–1318, Nov. 2019.
[105] E. A. Bastos, C. Meira Amaral da Luz, T. M. Oliveira, L. Ana Rodarte Rios, E. M. Vicente, and F. Lessa Tofoli, "A curve tracer for photovoltaic modules based on the capacitive load method," in *Proc. IEEE 15th Brazilian Power Electron. Conf. 5th IEEE Southern Power Electron. Conf. (COBEP/SPEC)*, Dec. 2019, pp. 1–6.
[106] M. M. Mahmoud, "Transient analysis of a PV power generator charging a capacitor for measurement of the I–V characteristics," *Renew. Energy*, vol. 31, no. 13, pp. 2198–2206, 2006.
[107] T. H. Warner and C. H. Cox, "A high power current-voltage curve tracer employing a capacitive load," *Sol. Cells*, vol. 7, nos. 1–2, pp. 175–181, Nov. 1982.
[108] S. Bifaretti, V. Iacovone, L. Cina, and E. Buffone, "Global MPPT method for partially shaded photovoltaic modules," in *Proc. IEEE Energy Convers. Congr. Expo. (ECCE)*, Sep. 2012, pp. 4768–4775.
[109] F. Spertino, J. Ahmad, P. Di Leo, and A. Ciocia, "A method for obtaining the I-V curve of photovoltaic arrays from module voltages and its applications for MPP tracking," *Sol. Energy*, vol. 139, pp. 489–505, Dec. 2016.
[110] M. Herman, M. Jankovec, and M. Topič, "Optimal IV curve scan time of solar cells and modules in light of irradiance level," *Int. J. Photoenergy*, vol. 2012, Dec. 2012, Art. no. 151452.
[111] J. Polo, W. G. Fernandez-Neira, and M. C. Alonso-García, "On the use of reference modules as irradiance sensor for monitoring and modelling rooftop PV systems," *Renew. Energy*, vol. 106, pp. 186–191, Jun. 2017.
[112] Y. Zhu and W. Xiao, "A comprehensive review of topologies for photovoltaic I–V curve tracer," *Sol. Energy*, vol. 196, pp. 346–357, Jan. 2020.
[113] J. K. Sayyad and P. S. Nasikkar, "An overview of methods used for outdoor performance characterisation of photovoltaic module string up to 10 kWp," *Int. J. Instrum. Technol.*, vol. 2, no. 2, pp. 114–134, 2019.
[114] E. Duran, M. Piliougine, M. S.-D. Cardona, J. Galán, and J. Andujar, "Different methods to obtain the I–V curve of PV modules: A review," in *Proc. 33rd IEEE Photovoltaic Spec. Conf.*, May 2008, pp. 1–6.
[115] J. K. Sayyad and P. S. Nasikkar, "Capacitor load based I–V curve tracer for performance characterisation of the solar photovoltaic system," *Appl. Sol. Energy*, vol. 56, no. 3, pp. 168–177, 2020.
[116] M. Cáceres, A. Firman, J. Montes-Romero, A. R. G. Mayans, L. H. Vera, E. F. Fernández, and J. D. L. C. Higueras, "Low-cost I–V tracer for PV modules under real operating conditions," *Energies*, vol. 13, no. 17, p. 4320, 2020.
[117] F. Spertino, J. Ahmad, A. Ciocia, P. D. Leo, A. F. Murtaza, and M. Chiaberge, "Capacitor charging method for I–V curve tracer and MPPT in photovoltaic systems," *Sol. Energy*, vol. 119, pp. 461–473, Sep. 2015.

[118] E. Skoplaki and J. A. Palyvos, "On the temperature dependence of photovoltaic module electrical performance: A review of efficiency/power correlations," *Sol. Energy*, vol. 83, no. 5, pp. 614–624, May 2009.
[119] Y. Erkaya, H. S. Illa, C. Conway, S. Dhali, and S. Marsillac, "Development of a string level fault detection system for solar tracking applications," in *Proc. IEEE 40th Photovoltaic Spec. Conf. (PVSC)*, Jun. 2014, pp. 3100–3103.
[120] F. Spertino and J. S. Akilimali, "Are manufacturing *I–V* mismatch and reverse currents key factors in large photovoltaic arrays?" *IEEE Trans. Ind. Electron.*, vol. 56, no. 11, pp. 4520–4531, Nov. 2009.
[121] E. Ortega, G. Aranguren, M. J. Saenz, R. Gutierrez, and J. C. Jimeno, "Photovoltaic module to module monitoring system," in *Proc. IEEE 7th World Conf. Photovoltaic Energy Convers. (WCPEC) (A Joint Conf. 45th IEEE PVSC, 28th PVSEC 34th EU PVSEC)*, Jun. 2018, pp. 2703–2708.
[122] J. Bai, Y. Cao, Y. Hao, Z. Zhang, S. Liu, and F. Cao, "Characteristic output of PV systems under partial shading or mismatch conditions," *Sol. Energy*, vol. 112, pp. 41–54, Feb. 2015.

JAVED SAYYAD received the bachelor's degree in electronics and telecommunication from the Maharashtra Institute of Technology (MIT), Pune, India, in 2013, and the master's degree from the Deogiri Institute of Engineering and Management Studies (DIEMS) at Aurangabad, Aurangabad, India, in 2016. He is currently pursuing the Ph.D. degree with the Photovoltaic Systems Laboratory, Symbiosis Institute of Technology, Symbiosis International (Deemed University), Pune. He also carries out research activities at the Photovoltaic Systems Laboratory, Symbiosis Institute of Technology, Symbiosis International (Deemed University), as a Senior Research Fellow (SRF). He has experience in electrical engineering, with an emphasis on photovoltaic systems, working mainly on the following topics, solar energy, monitoring systems, solar photovoltaic, power electronics, and the Internet of Things (IoT).

PARESH NASIKKAR received the bachelor's degree in instrumentation and control engineering from the Government College of Engineering (COE), Pune, India, in 2001, the M.Sc. degree in optoelectronics from Northumbria University, Newcastle upon Tyne, U.K., in 2004, and the Ph.D. degree in thin film solar photovoltaics based topic from the Northumbria Photovoltaic Applications Centre, Northumbria University, in 2009. From 2010 to 2011, he has worked as a Research Scientist (Research Innovation Technology Centre-Solar) with Thermax Ltd., Pune, and as a Solar Research Scientist (Solar Cells and Modules Research and Development) with SunEdison Research Private Ltd./ MEMC, Bangaluru, India, from 2011 to 2015. He is currently working as an Assistant Professor with the Department of Electronics and Telecommunication, Symbiosis Institute of Technology, Symbiosis International (Deemed University), Pune. He has experience in the energy area, emphasizing renewable energy, acting mainly in the following themes, thin-film semiconductor fabrication, solar PV materials for thin-film solar cells (TFSC), solar photovoltaic systems, and instrumentation.